Macromolecules

ARTICLE

pubs.acs.org/Macromolecules

Kinetics of Styrene Polymerization to Syndiotactic Polystyrene over Metallocene Catalyst on Flat Surface, Silica Nanotube Reactors and Porous Silica Particles

Sang Yool Lee,[†] Sung-Kyoung Kim,[‡] Thao M. Nguyen,[‡] Jin Suk Chung,[§,∥] Sang Bok Lee,[‡,⊥] and Kyu Yong Choi[†,*]

[†]Department of Chemical and Biomolecular Engineering, University of Maryland, College Park, Maryland 20742, United States

[‡]Department of Chemistry and Biochemistry, University of Maryland, College Park, Maryland 20742, United States

[§]School of Chemical Engineering and Bioengineering, University of Ulsan, Ulsan, Korea

[⊥]School of Nanoscience and Technology (WCU), Korea Advanced Institute of Science and Technology, Daejeon, Korea

ABSTRACT: The geometry of a catalyst support has a strong influence on the catalytic activity of heterogeneous metallocene catalysts for polymerization of α-olefins and styrene. In this study, the catalytic activities of $Cp^*Ti(OCH_3)_3$/MAO catalyst for styrene polymerization to syndiotactic polystyrene (sPS) have been investigated using three different types of support materials with different geometries: flat surface derived from a silicon wafer, cylindrical pores in silica nanotube reactor arrays, and random tortuous and interconnected pores in porous silica particles. With the same catalyst immobilization technique applied to these support materials, the highest titanium loading per unit support surface area has been obtained with a flat surface catalyst whereas porous silica particles of 15 nm average pore size has the lowest titanium loading per pore surface area. The metallocene catalyst supported on a flat silica surface also exhibited the highest catalyst activity per mole of titanium among different types of supported catalysts investigated in this study. The flat surface catalyst renders minimal mass transfer resistance for the catalytic components (metallocenes and MAO) as well as monomer and all the active sites are fully exposed to monomer and available for polymerization. The relatively low catalyst activity of the silica particle supported catalyst is attributed to the limited exposure of active sites to cocatalyst as well as monomer because of geometric obstructions. The catalyst deactivation kinetics for the different types of supported catalysts was very similar in the early stage of polymerization and fitted well by the first order deactivation kinetics with about 20 min of catalyst half-life. The sPS synthesized with all these supported catalysts show that sPS molecules assemble to a bundle of nanofibrils of about 30 nm in diameter.

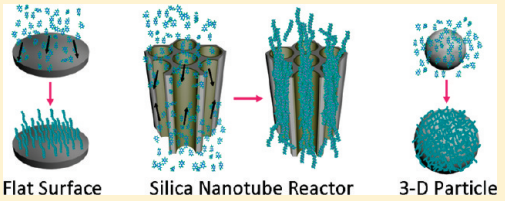

INTRODUCTION

Supported metallocene catalysts are widely used for the polymerization of α-olefins because the catalyst immobilized on a solid support can preserve the catalytic activity and provide desired polymer particle morphology. In industrial α-olefin polymerization processes, supported catalysts are used for slurry and gas phase polymerizations in stirred reactors, loop reactors, and fluidized bed reactors. Silica-supported metallocene catalysts used for olefin polymerization are interesting in that the silica fragmentation occurs during the polymerization and the characteristics of the fragmentation have a big impact on the catalyst activity, and resulting polymer properties and polymer particle morphology. Therefore, understanding the role of silica in supported metallocene and Ziegler−Natta catalysts is an important technical issue to design superior polymerization catalysts. Besides α-olefins, vinyl monomers such as styrene can also be polymerized over silica supported metallocene catalysts to syndiotactic polystyrene (sPS) with high syndiospecificity and high crystallinity. The polymerization of sPS with supported metallocene catalyts are advantageous over homogeneous catalyst systems in that the global gelation of sPS can be prevented by controlling the reaction rate and polymer morphology.[1,2] Syndiotactic polystyrene is an industrially important semicrystalline engineering polymer with strong chemical resistance, low dielectric constant, and high heat resistance suitable for harsh engineering applications in automotive, electrical, and electronics industries.[3,4]

One of the important issues in heterogeneously catalyzed polymerization processes is concerned with the characterization of catalytic activities for the design and optimization of industrial polymerization conditions and polymer properties control. However, the quantification of the intrinsic polymerization kinetics is known to be complex and difficult because of the presence of site heterogeneity and physical transport effects between the bulk fluid phase and the solid phase where active catalytic sites reside. The effects of support properties on the polymerization kinetics are not completely understood, either. The formation of active catalytic complex at the surface of the

Received: December 16, 2010
Revised: February 1, 2011
Published: February 28, 2011

support material such as silica gel is influenced by many factors such as local concentrations of the catalyst forming precursors, the structure and dimension of pores, and the structure of surface functional groups. For example, the presence of hydroxyl groups on the silica surface has a strong effect on the formation of active sites. Moreover, catalyst/polymer particle disintegration, interfacial and intraparticle mass and heat transfer effects can strongly affect the catalyst activity and the monomer composition in a heterogeneous catalyst particle.

The morphological development of polymer particles during the polymerization is also of great practical importance. The cracking and fragmentation of catalyst support materials with a buildup of polymers in the catalyst pores and subsequent polymer particle growth are the major mechanisms of complex morphological developments of polymer particles. For example, in silica-supported metallocene catalysts for ethylene polymerization, the buildup of hydraulic forces occurs within the pores at the beginning of polymerization, leading to the disintegration of silica particles that are loosely connected by polymers.

The catalytic activity is also strongly dependent on the catalyst preparation procedure that determines the chemical and physical states of the catalyst. Quite often, different catalytic performances are reported in the literature for the polymerization of α-olefins with the same or similar catalysts by different authors and direct comparison of catalyst performances is sometimes difficult. Therefore, interpretation of kinetic data obtained with a certain heterogeneous catalyst becomes catalyst specific. Even for the same catalyst constituents, the nature of the heterogeneous catalyst material and the way the active catalyst components are anchored and activated at the solid surface can dramatically change the catalytic behavior, often resulting in inconsistent kinetic behaviors and varying polymer properties (e.g., molecular weight distribution, copolymer composition, particle morphology, and density). The three most representative methods to support metallocene catalysts on to a silica are as follows: (i) direct immobilization of metallocene on a pretreated silica; (ii) reaction of MAO cocatalyst with the hydroxyl surface groups of the silica, and subsequent impregnation with a metallocene catalyst; (iii) immobilization of preactivated MAO/metallocene complex on a porous silica support.[5] The resulting catalyst activity is strongly affected by the catalyst preparation process.

The characterization of active catalytic species is also difficult because of heterogeneous nature of the catalyst. For example, the exact amount of transition metal sites active for polymerization is very hard to measure, and hence, the determination of intrinsic kinetic parameter values such as propagation rate constant and chain transfer constants is difficult.

Recently, some new approaches to synthesize supported catalysts have been reported for olefin and styrene polymerizations in the literature using nonconventional forms of silica materials.[6] Choi et al. used silica nanotube reactor arrays with a well-defined straight cyclindrical nanopores to polymerize styrene to sPS using $Cp^*Ti(OCH_3)_3$/MAO catalyst. They discovered that sPS grows as a bundle of nanofibrils through intertwining inside nanopores and surprisingly high molecular weight sPS was also obtained.[7] A flat silicon substrate covered by amorphous silica was also used to study the catalytic reaction and polymer morphology with chromium oxide catalyst for ethylene polymerization.[8−12]

In this paper, we report a new approach of studying heterogeneous polymerization kinetics using three different types of silica support geometries. To this purpose, we used the syndiospecific polymerization of styrene as a model system, and three well-defined catalyst support configurations: a hydroxylated silicon wafer (flat-surface catalyst), a silica nanotube reactor (cylindrical reaction tube), and a granular porous silica particle (3-dimensional support). A catalytic pore or channel in a silica nanotube reactor is straight whereas the pores in a silica particle are tortuous and pore size is not uniform. The flat surface catalyst and silica nanotube reactors are resistant to fragmentation whereas porous silica particle-supported catalyst with small pore diameters (∼15 nm) undergo particle fragmentation in the early stage of polymerization.[2,13] New experimental results with these supported catalysts are presented and analyzed using a simplified kinetic model.

EXPERIMENTAL SECTION

Materials. For the catalytic polymerization of styrene to syndiotactic polystyrene (sPS), styrene (Aldrich) monomer was vacuum distilled over calcium hydride, and activated alumina was used to remove inhibitors from the monomer. *N*-heptane (Fisher Scientific) was used as a diluent, and it was purified by being refluxed over sodium and benzophenone in nitrogen atmosphere. Trimethoxy (pentamethylcyclopentadienyl) titanium(IV) ($Cp^*Ti(OCH_3)_3$, Strem Chemicals, min 97%) and methylaluminoxane solution (MAO, Aldrich, 10 wt % in toluene) were used as catalyst and cocatalyst, respectively without further purification. Silicon wafer (University Wafer, P-type (100)), silica-coated anodized aluminum oxide films (SNTR200: Silica Nanotube Reactor, Anodisc 47, 200 nm pore diameter, Whatman; SNTR60: 60 nm pore diameter, prepared in author's laboratory (SBL)), and silica particles (Davisil, grade 643) were used as catalyst support materials.

Preparation of Supported Catalysts. The metallocene catalyst was supported on a flat surface using the following procedure. First, a silicon wafer was calcined at 250 °C for 24 h and then it was treated for 30 min in a solution of 30 vol % of hydrogen peroxide (Fisher, 30%) and 70 vol % of sulfuric acid (Fisher, +95%) to form hydroxyl groups on the surface, and it was washed with excess amount of deionized water. The acid-treated wafer was immersed in an MAO/toluene solution for 24 h, washed with toluene three times, and dried. The wafer was then immersed in a $Cp^*Ti(OCH_3)_3$ solution for another 24 h, washed with toluene, and finally dried in vacuo overnight. It was used as a flat-surface catalyst. The same procedure was used to support the catalyst onto silica particles.

For the preparation of catalytic silica nanotube reactors (SNTRs), anodized aluminum oxide (AAO) films with 200 and 60 nm diameter pores (SNTR200 and SNTR60) were treated as follows.[7] The nanopore surfaces of AAO films were coated with silica by surface sol−gel (SSG) method where an AAO film was first soaked in $SiCl_4$ (99.8%) solution.[14−22] They were then quickly immersed and washed with fresh hexane for 4 times to remove unabsorbed $SiCl_4$. The top surface of the AAO film was gently polished mechanically, and the AAO films were placed in a methanol/hexane (1:1 v/v) mixture, washed, and dried with nitrogen gas. This procedure was repeated several times to obtain 3−7 nm thick layer of silica at the pore surfaces. Figure 1(a) shows the scanning electron microscopic (SEM) image of an AAO film with 60 nm diameter pores of length 8 μm and Figure 1b is the transmission electron miscroscopic (TEM) image of the silica nanotube reactors liberated from the AAO film after dissolving the alumina matrix.

$Cp^*Ti(OCH_3)_3$ catalyst has been anchored onto the MAO-treated SNTRs and silica particles using the same procedure used for the flat surface catalyst. The titanium loading on each supported catalyst was measured by inductively coupled plasma optical emission spectrometry (ICP-OES(ACTIVA, JY HORIVA)). The specific surface area and pore

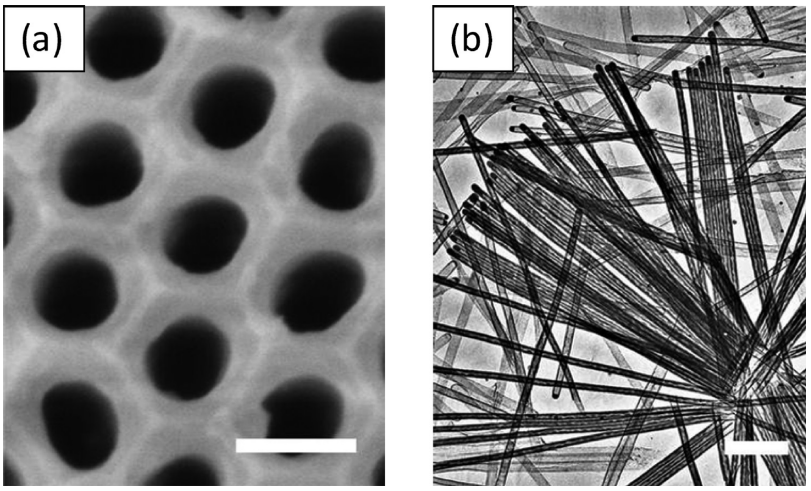

Figure 1. (a) SEM image of an AAO porous film with a pore diameter of 60 nm, (b) TEM image of silica nanotube reactors released after dissolving AAO. The scale bars are (a) 100 nm and (b) 1 μm.

Table 1. Properties of Supported Catalysts

catalyst system	[Ti] loading (mol-Ti/g-support)	specific surface area (m^2/g)	[Ti] loading (mol-Ti/m^2)	av pore size (nm)
flat surface catalyst	1.10×10^{-7}	1.464×10^{-3}	7.53×10^{-5}	n/a
SNTR (200 nm)	5.01×10^{-5}	2.3	2.18×10^{-5}	200
SNTR (60 nm)	1.42×10^{-4}	6.53	2.18×10^{-5} [a]	60
silica particles	4.33×10^{-4}	300	1.44×10^{-6}	15

[a] Assumed to be the same as SNTR200.

size were measured using BET method (Micromeritics, ASAP 2020) at the liquid nitrogen temperature using nitrogen as an adsorption gas. Before the measurement, the samples were degassed at 150 °C for 4 h to reach a final pressure of 10^{-4} Torr. The properties of these three supported metallocene catalysts are shown in Table 1. For SNTRs, the top surface of the film was mechanically polished to remove the catalyst and hence, the specific surface areas for the SNTRs in Table 1 represent the net pore surface areas where the catalyst is deposited.

The titanium loading on the silica particles (1.44×10^{-6} mol-Ti/m^2) used in this study is quite comparable to those reported in the literature for $Ti(OBu)_4$/MAO/SiO_2 catalyst (1.76×10^{-6} mol/m^2).[13] Table 1 indicates that titanium loading per surface area available for the catalyst deposition is largest for the flat-surface catalyst whereas the silica particles have the smallest surface loading of Ti. It is probably because the silica particle consists of very narrow pores distributed from 1 to 20 nm and small pores may restrict the access of MAO and catalyst. The pores of smaller than 10 nm in the silica particles used in this study (Davisil 643) account for about 20% of its total pore volume.

Although the characterization of dormant and active species in a heterogeneous metallocene catalyzed polymerization is very difficult, if not impossible, it is well-known that high activity of metallocene catalysts are imparted by MAO that forms a complex with the catalyst. Thus, it is important to have a heterogeneous catalyst structure that allows for the resistance-free transport of MAO molecules from the fluid phase to the catalytic site in narrow pores of a support material. MAO has a three-dimensional cage structure with four-coordinate aluminum centers bridged by three-coordinate oxygen atoms.[23] In general, MAO is present in oligomeric forms ($[AlOMe]_n$) of different size. The most stable structure in the temperature range between 75 and 300 °C is known to be MAO-12.[23] Figure 2a shows the structure of MAO-12 and Figure 2b is the MAO-12 structural image obtained using Accelrys Materials Studio Visualizer. The top view of MAO-12 shown in Figure 2c indicates that the largest dimension of the MAO-12 oligomer is 0.96 nm.

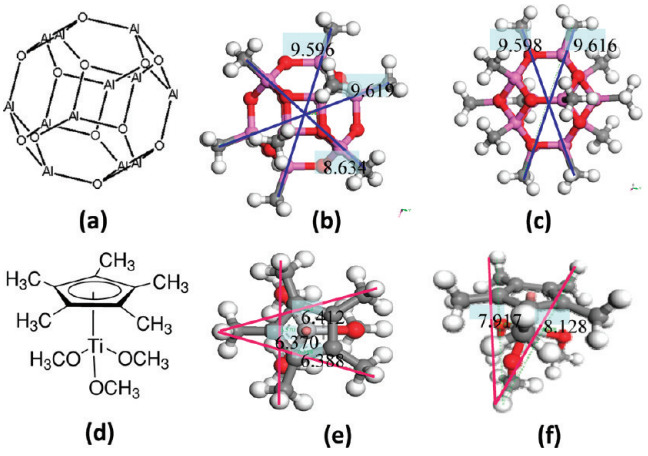

Figure 2. (a) MAO-12, (b) top view of MAO-12, (c) side view of MAO-12, (d) $Cp^*Ti(OCH_3)_3$ catalyst, (e) top view of $Cp^*Ti(OCH_3)_3$ catalyst, (f) side view of $Cp^*Ti(OCH_3)_3$ catalyst (units in Å).

The molecular structure and dimension of the catalyst ($Cp^*Ti(OCH_3)_3$) in Figure 2, parts e and f, show that the catalyst dimension is about 0.82 nm. The structural dimension of the catalyst and MAO-12 suggests that the dimension of the catalyst−MAO complex will be large and also, the fraction of pores in silica particles might not be large enough for the MAO oligomers to diffuse from the bulk liquid phase into small pores and complex with $Cp^*Ti(OCH_3)_3$ catalyst at the pore surface.

When MAO is immobilized on a silica calcined at 250 °C, the average pore diameter decreases by 18−35%, indicating that the reduced pore size due to MAO deposition can obstruct the access of metallocene catalyst and additional MAO or alkyls that are needed to activate the

dx.doi.org/10.1021/ma1028592 |*Macromolecules* 2011, 44, 1385–1392

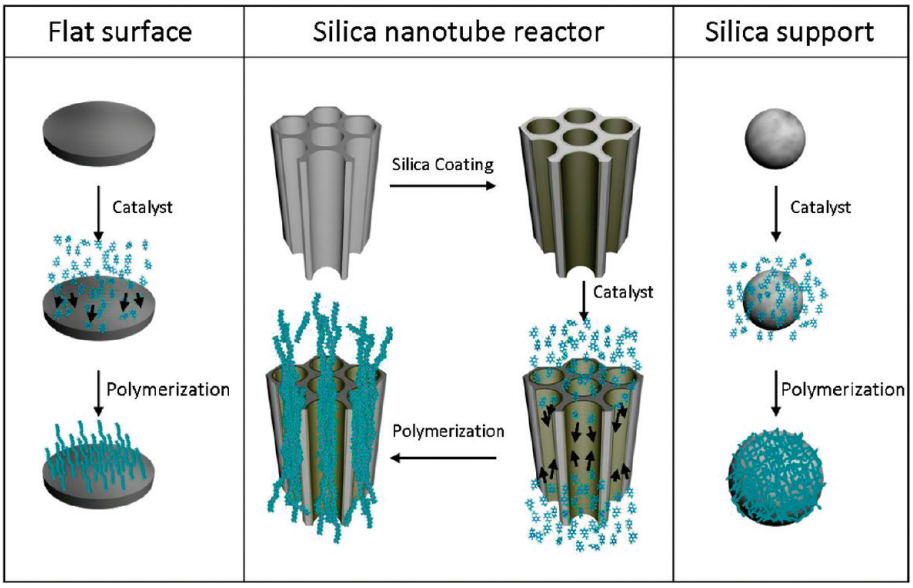

Figure 3. Polymerization of styrene over supported catalysts of three different geometries.

supported catalyst.[23] If we assume that a monolayer of MAO-12 and $Cp^*Ti(OCH_3)_3$ complex is formed on the silica surface and that the molecular dimensions of MAO-12 and catalyst shown in Figure 2 are used, the calculated pore diameter of silica decreases from 15 nm to about 11 nm, which is a 27% decrease from the size of untreated silica pores. This approximate calculation result agrees well with the literature report of 18−35% reduction in pore size after MAO treatment.[26] Moreover, if we consider the possibility of a multilayer adsorption of MAO, it is expected that some silica pores can be blocked more than 27%, severely limiting the diffusional access of catalyst and cocatalyst components. All these effects are expected to contribute to low titanium loadings per surface area and reduced catalytic activity in porous silica. In particular, the reduced access of bulky MAO cocatalyst can have a significantly adverse effect on the catalyst activation. In other words, the large surface area of silica may not be fully utilized for catalyst support, and not all the titanium sites may be catalytically active for the subsequent polymerization.

It is also possible that more surface silanol groups are left unused in the small diameter pores of silica particles after MAO is grafted onto the pore surface. When silica is calcined at 250 °C, the surface hydroxyl group concentration is about 2.4−3.2 mmol/g and the silica surface consists of mostly germinal and vicinal groups and some isolated silanol groups.[26] A relatively large concentration of silanol groups in the promixity can promote the formation of inactive catalytic sites.[6] It is also interesting to note that the titanium loading (mol-Ti/m^2) for three-dimensional silica particles is only 1.9% of the titanium loading for a flat surface catalyst, suggesting that the efficiency of metallocene immobilization onto a silica support is quite low for the silica particles.

Polymerization of Styrene. Polymerization of styrene to sPS with each supported catalyst was carried out using small glass reactors at 70 °C. The reaction vessel was charged with desired amounts of purified monomer and *n*-heptane, supported $Cp^*Ti(OCH_3)_3$ catalyst, and MAO in an argon-filled glovebox. The MAO concentration in a liquid phase was kept constant at 5.0 wt % (0.072 mol/L) in all the experiments with flat-surface catalyst and SNTRs. The MAO concentration was slightly higher for silica-supported catalysts (7.87 wt % or 0.112 mol/L). The charged reaction vessel was immersed in a constant temperature bath and the polymerization was carried out at 70 °C for 15−240 min. After polymerization, the mixture was washed with an acidified methanol solution (10% hydrochloric acid) to remove MAO residue, then washed again with excess amount of methanol, and finally dried in vacuo. Figure 3 illustrates the schematics of the flat-supported catalyst, silica nanotube reactors, and conventional silica particle supported catalyst for syndiospecific styrene polymerization. The syndiotacticity of sPS measured by extraction with boiling methyl ethyl ketone (MEK) or ^{13}C NMR spectroscopy was 95−100% for the tested catalysts. The sPS analysis data of syndiotacticity and molecular weight distribution with $Cp^*Ti(OCH_3)_3$ /MAO catalyst system have been reported previously in detail elsewhere.[7,27,28]

RESULTS AND DISCUSSION

Polymer Morphology. sPS is known to grow in nanofibrillar morphology with silica-supported metallocene catalysts.[2,7] Figure 4 shows the SEM images of sPS growing from three different supported catalysts. All these SEM photos show that indeed sPS grows as nanofibrils regardless of the support type. For the flat surface catalyst, sPS nanofibrils of about 30 nm-diameter grow in a direction normal to the catalytic surface. Figure 4a1 shows the top view of the sPS nanofibrils grown on the flat surface catalyst. In the SNTRs, the sPS extruded out from nano pores. Parts b1 and b2 of Figure 4 show that the top surface of SNTRs is covered with 30−50 nm sPS nanofibrils extruded out from the pores. Similar sPS nanofibrils are also seen in the polymer particles from silica-supported catalysts (Figure 4, parts c1 and c2). Polymerization of olefins with silica-supported metallocene catalyst are well-known to exhibit a gradual fragmentation of catalyst/polymer particles and particle shape-replication phenomena. The fragmentation of a silica-supported catalyst particle starts in the surface region which is quickly covered with polymer layer, causing a diffusion barrier for monomer. As monomers diffuse and polymerize inside the particle, the silica core gradually disintegrates and expose catalytic sites.[5,25] Similar catalyst fragmentation and shape replication phenomena occur in sPS polymerization with $Cp^*Ti(OCH_3)_3$/MAO/silica catalyst.[2] Figure 4c1 shows a residue of a relatively large unfragmented silica particle of about 5 μm size embedded in the matrix of sPS nanofibrils. It is likely that titanium sites buried in this incompletely fragmented silica particle were not accessible by monomer and hence not used forpolymerization. The stress fibrils are

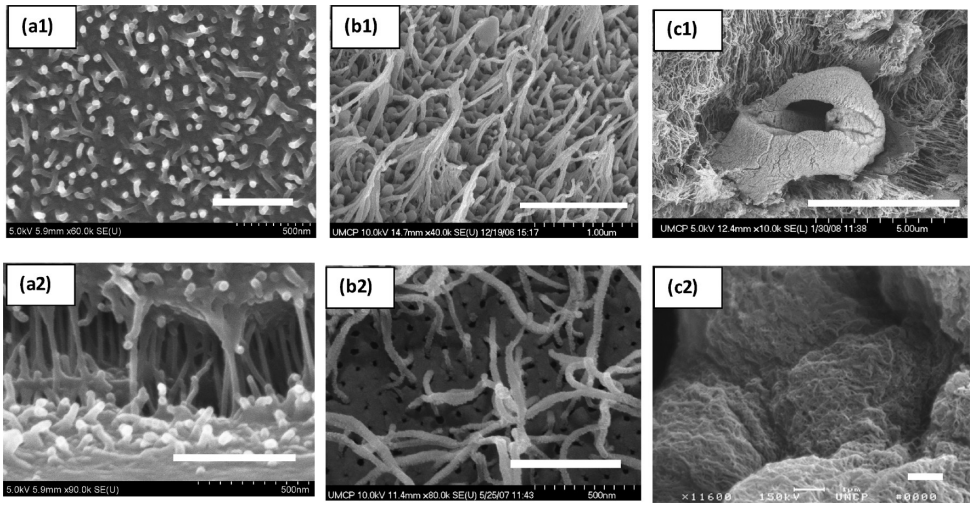

Figure 4. SEM images of sPS nanofibrils: (a1, a2), flat surface catalyst; (b1, b2), SNTR 200 and SNTR60; (c1, c2), porous silica particle catalyst. Scale bars: (a1) 500 nm, (a2) 500 nm, (b1) 1.0 μm, (b2) 500 nm, (c1) 5 μm, and (c2) 1.0 μm.

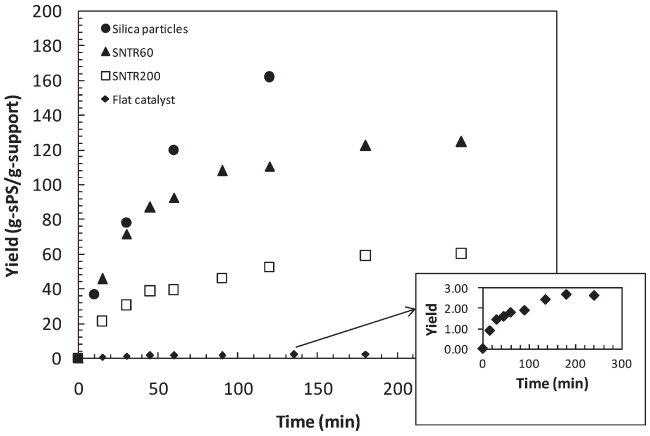

Figure 5. Polymer yield vs reaction time with three different supported catalysts.

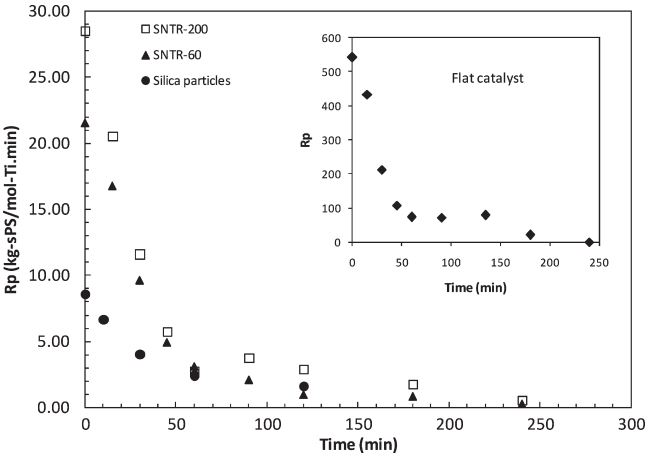

Figure 6. Catalyst activities for styrene polymerization for different supported catalysts.

also visible in Figure 4c1, clearly indicating that they were formed by the disintegration of silica particles during the polymerization.

Catalyst Activity. For the three supported catalyst systems of different geometry used in this study, polymer yield (g-sPS/g-support) vs reaction time data are shown in Figure 5. Each data point represents an independent polymerization experiment. Since the specific surface area (m^2/g) of a flat surface catalyst is the smallest of the three different support geometry, the polymer yield per gram of support is smallest for the flat-surface supported catalyst. It is observed that the polymer yield with small pore silica nanotube reactor (SNTR60) is quite comparable to that of silica particle-supported catalyst (average pore diameter =15 nm) up to about 20 min.

From the polymer yield data shown in Figure 5, the instantaneous polymerization rates in kg-polymer/mol-Ti·min were calculated by numerically differentiating the polymer yield data and the results are shown in Figure 6. Notice that the catalyst activity is now the highest for the flat-surface catalyst and the lowest for the three-dimensional silica particle-supported catalyst. The activities of the silica nanotube reactors (SNTR200 and SNTR60) are quite similar and they lie between those for the two other catalyst geometries (flat-surface and spherical particles). The initial activity of the flat-surface catalyst is nearly 550 kg/mol-Ti·min (inset) that is about 70 times larger than that of the silica particle-supported catalyst. The reduced activity of the flat surface catalyst after 60 min of reaction is still far higher than those for other supported catalysts. Figure 6 suggests that the more open structure of the catalyst support (e.g., flat-surface catalyst) is, the higher the specific catalyst activity or polymerization rate becomes. In other words, the geometry of a catalyst support is an important factor that affects the catalytic activity for sPS polymerization.

Figure 6 also shows that all these supported catalyst systems used in our study exhibit decay type kinetic profiles. Such kinetic profiles have been commonly observed in heterogeneous metallocene or Ziegler−Natta catalyzed polymerization of α-olefins and styrene. The exact mechanism of gradual decline of catalytic activity in these systems is not completely understood but it is generally attributed to the catalyst deactivation caused by, for example, the loss of active sites by impurities, the interaction with support surfaces, spontaneous site deactivation, and the restrictions of the monomer access to the active sites via mass transfer limitations.

dx.doi.org/10.1021/ma1028592 |*Macromolecules* 2011, 44, 1385–1392

Table 2. Initial Catalyst Activities

	$\tilde{R}_{p0}$ (g/gcat·min)	R_{p0} (g/mol-Ti·min)	$[M]_b$ (mol/L)	$\eta_0\Psi_0k_p$ (L/mol·min)	$(\eta_0\Psi_0)/(\eta_0\Psi_0)_{flat}$
flat catalyst	0.0594	5.40×10^5	4.99	1.04×10^3	1.0
SNTR (200 nm)	1.423	2.84×10^4	4.99	54.70	0.053
SNTR (60 nm)	3.056	2.15×10^4	4.99	41.43	0.040
silica particle	3.672	8.48×10^3	4.85	16.81	0.016

In Figure 6, we also observe that the initial catalyst activities for the four supported catalyst systems show quite significant differences. In our experiments, the first samples for the yield measurements were taken at t = 15 min because it was very difficult to take the samples earlier than 15 min and secure sufficient amount of polymer sample for analysis. Table 2 summarizes the initial polymerization rate data.

Polymerization Rate Analysis. To understand the observed rate phenomena for the supported catalyst systems, let us consider the polymerization rate (g/gcat·min) that can be expressed as

$$\tilde{R}_p = k_p[\mathrm{M}]_p f([\mathrm{Ti}])w_m \quad (1)$$

where k_p is the propagation rate constant (L/mol·min), $[\mathrm{M}]_p$ is the monomer concentration (mol/L) at the catalytic site, w_m is the molecular weight of monomer (g/mol), [Ti] is the active catalyst site concentration (mol-Ti/g-cat). The dependence of the polymerization rate on the catalyst site concentration (i.e., $f([\mathrm{Ti}])$) is expressed as a functional form in eq 1 because not every titanium site may be catalytically active. The intrinsic catalyst activity represented by eq 1 is affected by catalytic site deactivation and monomer diffusion resistance because of the heterogeneous nature of the polymerization.

To account for the monomer mass transfer resistance to active catalytic sites through a polymer, we introduce a parameter η as the effectiveness factor, i.e., $[\mathrm{M}_p] = \eta[\mathrm{M}]_b$ where $[\mathrm{M}]_b$ is the bulk phase monomer concentration. It is expected that monomer diffusion effect is minimal for a flat-surface catalyst system whereas the silica-supported catalyst can have larger pore diffusion resistance for styrene monomer because the pore diameter is very small, tortuous, interconnected, and buried deep inside a particle covered with polymer. For the flat-surface catalyst, all the active sites are likely to be fully exposed to monomer and we expect that the polymerization would takes place at almost every titanium site immobilized on the support surface. It is also expected that spherical silica particles will undergo particle fragmentation during the polymerization[1,2] whereas no such fragmentation is expected in SNTRs, because the long cylindrical pores are fairly far separated by alumina matrix.

Since not all the titanium sites may be catalytically active for styrene polymerization and the activity may also change with time, we define a new catalyst activity parameter (ψ) that accounts for the catalytic efficiency of the initial titanium loading for polymerizaton. In other words, $\Psi[\mathrm{Ti}]_0$ represents the catalyst site efficiency based on the initial titanium concentration on the support surface. Both η and ψ are the empirical parameters because they are difficult to measure experimentally. Then, eq 1 can be recast into the following form using these newly defined parameters:

$$\tilde{R}_p = k_p(\eta[\mathrm{M}]_b)(\psi[\mathrm{Ti}]_0)w_m \quad (2)$$

If we assume that the loss of catalyst activity (deactivation) occurs with time and that it can be modeled by the first-order decay kinetics, eq 2 can be written as

$$\tilde{R}_p = k_p(\eta[\mathrm{M}]_b)(\psi_0[\mathrm{Ti}]_0e^{-k_dt})w_m \quad (3)$$

where k_d is the deactivation rate constant and ψ_0 is the initial catalyst activity parameter. Here, it should be pointed out that the assumption of the first order deactivation kinetics is an approximation because detailed deactivation mechanisms are not exactly understood for this type of catalyst. The first order deactivation kinetics have been widely employed in modeling the olefin polymerization kinetics with heterogeneous transition metal catalysts including metallocene catalysts.

Here, the polymerization rate can also be conveniently expressed in g/mol-Ti·min (i.e., R_p=$\tilde{R}_p/[\mathrm{Ti}]_0$). Then, from eq 3, the initial polymerization rate in g/mol-Ti·min can be expressed as

$$R_{p0} \equiv \frac{\tilde{R}_{p0}}{[\mathrm{Ti}]_0} = \eta_0\psi_0k_p[\mathrm{M}]_bw_m \quad (4)$$

where η_0 is the initial effectiveness factor. For the experimental conditions used in this study, the monomer concentration remains nearly constant because the total polymer yield was very low (i.e., $[\mathrm{M}]_b \approx$ constant)). If we normalize the polymerization rate (g/mol-Ti·min) with initial polymerization rate, we obtain the following equation:

$$\frac{R_p}{R_{p0}} = \frac{\eta}{\eta_0}\exp(-k_dt) \quad (5)$$

In Figure 6, we observe that catalyst activities decline rapidly to very low values after about 60 min. In our experiments, the accuracy of measurements of polymerization rates was much higher during the early period of polymerization (e.g., $0 < t < 60$ min) where polymer yield change with reaction time was quite large (Recall that the catalyst activity was determined by numerically differentiating the polymer yield data with respect to time.). Therefore, to test the validity of eq 5, we used the rate data for the first 60 min of reaction. Figure 7 shows a plot of $-\ln(R_p/R_{p0})$ vs reaction time (t) (eq 5) for all the catalysts used in our study. It is quite interesting to note that the rate data for four different supported catalysts are reasonably well fitted up to about 30 min of reaction time by a single straight line, suggesting that the first-order deactivation model is justifiable for this time period. It should be pointed out that the reaction rate data for the silica particle-supported catalyst start to deviate from the linear fit after about 30 min. From Figure 5, the polymer yield at 30 min is 80 g/g-catalyst for the silica particle-supported catalyst. If 50 μm is taken as a mean silica particle diameter at t = 0, the corresponding polymer particle size after 30 min reaction is calculated from the yield data to be about 210 μm. Although this calculation is approximate, with this large particle growth factor, it is likely that the intraparticle monomer diffusion resistance can be significant in 3-dimensional silica particles. In other words, with the growth of polymer particles, the intrinsic deactivation kinetics observed during the polymerization after 30 min will be masked by the

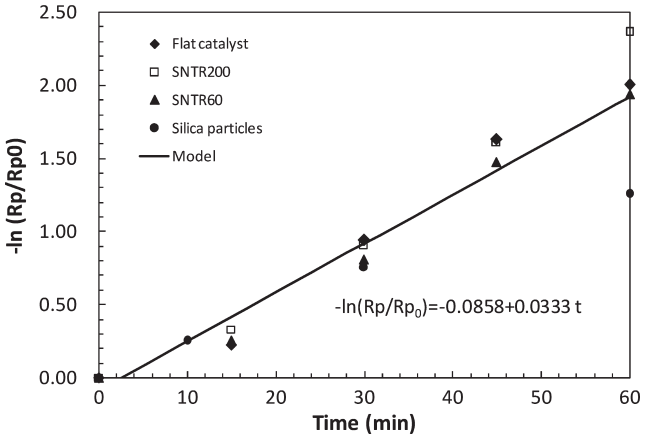

Figure 7. Test of first order catalyst deactivation model.

physical transport process. The deactivation parameter (k_d) estimated from the slope of the straight line in Figure 7 is 0.033 min^{-1} and the corresponding catalyst half-life is about 20 min. Also, we find that the value of η/η_0 is 1.09, indicating that the effectiveness factor is practically constant during first 20−30 min of polymerization.

At this point, let us go to Table 2 again to further analyze the experimentally observed initial polymerization rate data for different types of supported catalysts. The last column in Table 2 shows the ratio of the initial catalyst efficiency parameters for the SNTRs and silica-supported catalyst with respect to that of flat-surface catalyst. This simple analysis indicates that the catalyst efficiency factors for SNTRs and silica particles are only about 1.6−5.3% of the catalyst efficiency factor for the flat surface catalyst. Since $\eta/\eta_0 \approx 1.0$ during the early reaction period, we can say that ψ/ψ_0 = 0.016−0.053 for the SNTRs and silica particles. In other words, if we assume that extent of monomer diffusion resistance in each supported catalyst is similar (e.g., before diffusion resistance becomes severe in silica particle-supported catalyst), then this ratio can be approximated as the ratio of the fraction of active sites effective for the polymerization. The geometrically constrained pores in SNTRs and silica particles have substantially low usage of titanium catalyst deposited onto the pore surfaces. It is possible that surface properties and the geometrical constraints in the SNTRs and silica particles might have influenced the formation of active titanium catalyst sites. As mentioned earlier, the diffusion of MAO into the pores during the catalyst preparation (for anchoring the catalyst) and during the polymerization (as cocatalyst) might have been very ineffective, resulting in the low usage of metallocene catalyst. When a silica-supported chromium oxide catalyst (Phillips-type catalyst) is used for ethylene polymerization, typically less than 10% of the chromium atoms are believed to be active.[11] This results suggest that the use of flat surface catalysts offers a new technique to measure the intrinsic kinetics of catalytic polymerization and to help design better support materials.

CONCLUDING REMARKS

The kinetics of catalytic polymerization of styrene to syndiotactic polystyrene has been investigated using flat wafer, anodized alumina film, and porous silica gel particle as support materials for $Cp^*Ti(OCH_3)_3$/MAO catalyst. The same catalyst supporting technique was used for the comparison of resulting catalytic performances, particularly polymerization rate characteristics. The catalyst loading per support surface area and the corresponding catalyst activity are strongly influenced by the geometries of support materials. The flat-surface catalyst has been found to have the largest titanium loading per area and the highest catalyst activity per mole of titanium. A kinetic model analysis indicates that the active titanium sites for the SNTRs and silica particles are less than 10% of those for the flat-surface catalyst. It implies that the pore dimensions and support characteristics have a significant impact on the catalyst performance for sPS polymerization. The deactivation kinetics for these supported catalyst systems were well fitted by the decay type kinetic model during the early period of polymerization. All these supported catalysts yield sPS as nanofibrils of about 30 nm-diameters. Finally, similar support effects are expected in α-olefin polymerization and our forthcoming paper will report the experimental results.

Notes

[‖] On leave from University of Ulsan.

ACKNOWLEDGMENT

S.B.L. thanks the WCU program funded by the KOSEF under the MEST (Grant Number: R31-2008-000-10071-0).

REFERENCES

(1) Han, J. J.; Lee, H. W.; Yoon, W. J.; Choi, K. Y. *Polymer* **2007**, *48*, 6519–6531.
(2) Han, J. J.; Yoon, W. J.; Lee, H. W.; Choi, K. Y. *Polymer* **2008**, *49*, 4141–4149.
(3) Malanga, M. Syndiotactic polystyrene materials. *Adv. Mater.* **2000**, *12*, 1869–1872.
(4) Schellenberg, J.; Leder, H.-J. *Adv. Polym. Technol.* **2006**, *25*, 141–151.
(5) Fink, G.; Steinmetz, B.; Zechlin, J.; Przybyla, C.; Tesche, B. *Chem. Rev.* **2000**, *100*, 1377–1390.
(6) Silveira, F.; Alves, M. d. C. M.; Stedile, F. C.; Pergher, S. B.; Rigacci, A.; Santos, J. H. Z. d. *J. Mol. Catal A: Chem.* **2009**, *298*, 40–50.
(7) Choi, K. Y.; Han, J. J.; He, B.; Lee, S. B. *J. Am. Chem. Soc.* **2008**, *130*, 3920–3926.
(8) Thüne, P. C.; Loos, J.; de Jong, A. M.; Lemstra, P. J.; Niemantsverdriet, J. W. *Top. Catal.* **2000**, *13*, 67–74.
(9) Thüne, P. C.; Loos, J.; Wouters, D.; Lemstra, P. J.; Niemantsverdriet, J. W. *Macromol. Symp.* **2001**, *173*, 37–52.
(10) Han, W.; Müller, C.; Vogt, D.; Niemantsverdriet, H.; Thüne, P. C. *Macromol. Rapid Commun.* **2006**, *27*, 279–283.
(11) van Kimmenade, E. M. E.; Loos, J.; Niemantsverdriet, J. W.; Thüne, P. C. *J. Catal.* **2006**, *240*, 39–46.
(12) Andoni, A.; Chadwick, J. C.; Milani, S.; Niemantsverdriet, H.; Thüne, P. C. *J. Catal.* **2007**, *247*, 129–136.
(13) Soga, K.; Nakatani, H. *Macromolecules* **1990**, *23*, 957–959.
(14) He, B.; Kim, S. K.; Son, S. J.; Lee, S. B. *Nanomedicine* **2010**, *5*, 77–88.
(15) Yu, J.; Bai, X.; Suh, J.; Lee, S. B.; Son, S. J. *J. Am. Chem. Soc.* **2009**, *131*, 15574–15575.
(16) Kim, S.-K.; Lee, S. B. *J. Mater. Chem.* **2009**, *19*, 1381–1389.
(17) Nan, A.; Bai, X.; Son, S. J.; Lee, S. B.; Ghandehari, H. *Nano Lett.* **2008**, *8*, 2150–2154.
(18) Bai, X.; Son, S. J.; Zhang, S.; Liu, W.; Jordan, E. K.; Frank, J. A.; Venkatesan, T.; Lee, S. B. *Nanomedicine* **2008**, *3*, 163–174.
(19) He, B.; Son, S. J.; Lee, S. B. *Anal. Chem.* **2007**, *79*, 5257–5263.
(20) Son, S. J.; Lee, S. B. *J. Am. Chem. Soc.* **2006**, *128*, 15974–15975.
(21) Son, S. J.; Reichel, J.; He, B.; Schuchman, M.; Lee, S. B. *J. Am. Chem. Soc.* **2005**, *127* (20), 7316–7317.
(22) Jayaraman, K.; Okamoto, K.; Son, S. J.; Luckett, C.; Gopalani, A. H.; Lee, S. B.; English, D. S. Observing capillarity in hydrophobic silica nanotubes. *J. Am. Chem. Soc.* **2005**, *127*, 17385–17392.

(23) Zurek, E.; Ziegler, T. *Prog. Polym. Sci.* **2004**, *29*, 107–148.
(24) Alexiadis, A.; Andes, C.; Ferrari, D.; Korber, F.; Hauschild, K.; Bochmann, M.; Fink, G. *Macromol. Mater. Eng.* **2004**, *289*, 457–466.
(25) Knoke, S.; Korber, F.; Fink, G.; Tesche, B. *Macromol. Chem. Phys.* **2003**, *204*, 607–617.
(26) Smit, M.; Zheng, X.; Loos, J.; Chadwick, J. C.; Koning, C. E. *J. Polym. Sci., Part A: Polym. Chem.* **2005**, *43*, 2734–2748.
(27) Ishihara, N.; Seimiya, T.; Kuramoto, M.; Uoi, M. *Macromolecules* **1986**, *19*, 2464–2465.
(28) Huang, B.; Cao, K.; Li, B. G.; Zhu, S. P. *J. Appl. Polym. Sci.* **2004**, *94*, 1449–1455.